Remote Sensing of Environment 251 (2020) 112081

Contents lists available at ScienceDirect

Remote Sensing of Environment

journal homepage: www.elsevier.com/locate/rse

Improving precision of high-rate altimeter sea level anomalies by removing the sea state bias and intra-1-Hz covariant error

Fukai Peng[a,b,c,*], Xiaoli Deng[b]

[a] School of Geospatial Engineering and Science, Sun Yat-Sen University, Guangzhou 510275, China
[b] School of Engineering, The University of Newcastle, University Drive, Callaghan, NSW 2308, Australia
[c] Southern Marine Science and Engineering Guangdong Laboratory (Zhuhai), Zhuhai 519082, China

ARTICLE INFO

Keywords:
Satellite altimetry
Sea level anomaly
Jason missions
Sentinel-3A
Data precision
Australian coastal zone
Sea state bias
Intra-1-Hz covariant error

ABSTRACT

This paper assessed the precision of 20-Hz sea level anomaly (SLA) estimates with different sea state bias (SSB) corrections from reprocessed Jason-1/2/3 and Sentinel-3A data over the period of 2002–2019 within 100 km from the entire Australian coast. The altimeter waveforms were retracked by the modified Brown-peaky (MBP) retracker for Jason missions and by the SAMOSA+ retracker for Sentinel-3A. We recalculated the 20-Hz and composite SSB corrections using a regional parametric model from 20-Hz retracked estimates of the SLA, significant wave height (SWH) and wind speed. The composite SSB correction, which was recomputed after removing the retracker-dependant correlated error in 20-Hz SLA, is found to achieve better performance than other SSB corrections in the study area. Applying the 20-Hz and composite SSB corrections has reduced ~10% and ~13% of noise, respectively, in the MBP-retracked 20-Hz Jason SLA estimates, while only ~2% of noise reduction is shown by applying the 1-Hz standard SSB correction. It is also found that the improvement of retracked Sentinel-3A SLA estimates by SSB corrections is very low (~3%), indicating a dedicated SSB correction model should be developed for the SAR mode altimeter.

As a result, the precision of composite SSB-corrected SLA estimates for all Jason missions can be retained at the level of 5.1 ± 1.1 cm until 3 km from the Australian coast, which is slightly lower than that of Sentinel-3A (4.2 ± 0.9 cm). The degradation within 3 km from the coast mainly corresponds to the along-track direction for MBP-retracked Jason SLA estimates, and the across-track direction for SAMOSA+ retracked Sentinel-3A SLA estimates, respectively.

1. Introduction

The high-rate (e.g., 20-Hz) altimeter sea level anomaly (SLA) estimates from multi-altimetry missions are of great interest for studying small-scale ocean dynamics and bathymetry (Birol and Delebecque, 2014; Bouffard et al., 2011; Sandwell et al., 2006). In coastal areas the high-rate SLA can get closer to the coast without land contamination (Gommenginger et al., 2011). These data are now available in the last 10 km to the coast thanks to the efforts made in the last two decades including advanced coastal waveform retracking techniques, improved orbit solutions, range and geophysical corrections (e.g., Passaro et al., 2014; Peng and Deng, 2018a; Cipollini et al., 2017a). However, the precision of high-rate altimeter SLA estimates still needs to be quantified in order to guarantee the reliability of this dataset.

In this study, we focus on quantifying the improved precision of high-rate SLA estimations in Australian coastal zones via a study of the retracker-dependent sea state bias (SSB) and intra-1-Hz corrections. Such information is required in order to correctly understand the recent and future sea-level change, interpret coastal erosion and model shallow water tides (e.g., Deng et al., 2011; Seifi et al., 2019; Karimi et al., 2019).

The SSB correction compensates the bias between altimeter-observed sea surface height (SSH) and mean sea level within the altimeter footprint. It includes three components: electromagnetic (EM) bias, skewness bias, and retracker bias (Gaspar et al., 1994). Of them, the retracker bias is affected not only by the sea states but also by the waveform retracking algorithm. The SSB correction varies from a few centimetres to a few decimetres depending on different sea states, and thus playing an important role in reducing SLA noise (Labroue et al., 2006). Because of the limited understanding of the mechanism that generates the SSB, the theoretical modelling of SSB correction is still challenging. As a result, the SSB correction is usually empirically

* Corresponding author at: School of Geospatial Engineering and Science, Sun Yat-Sen University, Guangzhou 510275, China.
E-mail addresses: pengfk@mail.sysu.edu.cn (F. Peng), xiaoli.deng@newcastle.edu.au (X. Deng).

https://doi.org/10.1016/j.rse.2020.112081
Received 29 January 2020; Received in revised form 10 August 2020; Accepted 31 August 2020
Available online 21 September 2020

modelled (Gaspar and Florens, 1998).

The SSB correction was firstly modelled as a function of significant wave height (SWH) due to strong dependency of SSB with SWH (Born et al., 1982). Later on, the altimeter-derived wind speed was introduced as the second variable in the empirical model to better describe the SSB correction (Chelton, 1994; Gaspar et al., 1994). Since then, non-parametric methods based on SWH and wind speed information have been proposed and proved to have better performance than the parametric algorithms (Gaspar and Florens, 1998; Labroue et al., 2006; Labroue et al., 2008; Tran et al., 2010a, 2010b; Tran et al., 2012; Vandemark et al., 2002). More recently, the studies showed that the use of mean wave period as the third variable can further improve the SSB correction (Pires et al., 2016; Tran et al., 2006).

The intra-1-Hz correction is to correct the correlated error between SWH and SLA estimates induced by the waveform retracking, which dominates the SLA noise at short wavelengths (Zaron and DeCarvalho, 2016). This error was firstly addressed by a two-pass retracking algorithm (Sandwell and Smith, 2005; Garcia et al., 2014). In the second-pass retracking, the smoothed along-track SWH was treated as a priori parameter to solve the range estimate, and thus reducing the correlated error. Zaron and DeCarvalho (2016) further investigated this small-scale error using collinear differences of SSH and SWH between Jason-1 and Jason-2, and developed an empirical correction based on the high-pass filtering of SWH. A recent study by Quartly et al. (2019) demonstrated that the error due to the correlation between high-rate SWH and SLA estimates can be reduced using the empirical correction based on a linear relationship between SWH and SLA estimates. The magnitude of the correction is, however, dependen upon the waveform retracker implemented.

Passaro et al. (2018) developed an SSB correction algorithm via a regional parametric model using 20-Hz altimeter SLA, SWH and wind speed estimates. Applying this regional SSB correction at 20-Hz resulted in a significant improvement on the SLA precision and a reduction in the correlation error between SLA and SWH estimates in the Mediterranean Sea and North Sea. However, the high-frequency noise caused by the SLA and SWH correlation may affect the modelling of SSB corrections, as the non-linearities of the ocean waves should not vary at scales smaller than 10 km (Quartly et al., 2019). Therefore, this motivates us to remove the correlated error before building the SSB correction and verify whether this would lead to the unification of SSB model for different altimeters used in this study.

Although these two corrections have successfully reduced the SLA noise for different conventional altimeters, their impacts on the latest synthetic aperture radar (SAR) mode altimeter (e.g., Sentinel-3A) could be different because of two reasons. First, the 20-Hz consecutive footprint of the SAR mode altimeter does not overlap with each other, which may result in a weak correlation between SWH and SLA estimates (Dinardo et al., 2018; Donlon et al., 2012; Labroue et al., 2012). Second, the footprint size in the along-track dimension is small (~300 m), therefore the long ocean waves (~600–700 m) cannot be fully imaged by the altimeter, leading to the degradation of SWH retrievals and then the SSB correction (Moreau et al., 2018). Therefore, it is important to evaluate the performance of these two corrections on the SAR mode altimeter.

We have recently generated the 20-Hz SLA datasets through retracking Jason altimeter waveforms in the period of 2002–2019 around Australia using the modified Brown-peaky (MBP) retracker developed by Peng and Deng (2020). Using these retracked Jason datasets together with Sentinel-3A data, the aim of this paper is to systematically investigate the SSB correction and quantify the intra-1-Hz correction for SLA estimates from different retrackers including the MBP retracker. The novelty of this paper compared to previous studies lies in that 1) it presents a strategy to separately solve the intra-1-Hz and SSB corrections; and 2) it brings together for the first time analysis of the precision of retracked high-rate SLA estimates from Jason and Sentinel-3A missions in Australian coastal zones, which will be valuable for both scientific and engineering applications.

The paper is organised as follows. The data and study region are presented in Section 2. The methods used for calculating the intra-1-Hz correction and SSB correction, as well as the methods to assess the precision of altimeter SLA estimates are shown in Section 3. Results are displayed and discussed in Section 4. The conclusions and important findings of this study are summarised in Section 5.

2. Data and study area

2.1. Altimeter dataset

The 20-Hz altimeter measurements from 16-year Jason missions and 3-year Sentinel-3A are used in this study. These include Jason-1 (cycles 1 to 259, January 2002 – January 2009), Jason-2 (cycles 1 to 303, July 2008 – September 2019), Jason-3 (cycles 1 to 84, February 2016 – May 2018) and Sentinel-3A (cycles 5 to 49, June 2016 – September 2019). The altimeter data of Jason missions are contained in the Sensor Geophysical Data Record (SGDR) product and are distributed through the website ftp.access.aviso.altimetry.fr, while the Sentinel-3A synthetic aperture radar (SAR) mode data are available in the SARvatore (SAR Versatile Altimetric Toolkit for Ocean Research and Exploitation) data repository https://wiki.services.eoportal.org/

Here, Jason and Sentinel-3A waveforms were respectively reprocessed by two dedicated coastal retrackers to retrieve range, SWH and sigma0 estimates in coastal areas. The first is the MBP retracker, which is developed to retrack the pulse-limited altimeter waveforms. Its superior performance to the official SGDR 4-parameter maximum likelihood estimator (MLE4) retracker has been demonstrated in the Australian coastal zone (Peng and Deng, 2020). The second is the SAR Altimetry Mode Studies and Applications+ (SAMOSA+) retracker developed for SAR waveforms, which works better than the SAMOSA retracker in the German Bight and West Baltic Sea (Dinardo et al., 2018; Fenoglio et al., 2019). For detailed description of MBP and SAMOSA+ retrackers, please refer to Peng and Deng (2020) and Dinardo et al. (2018). The estimated sigma0 was then translated into wind speed estimate using the Abdalla (2012) model.

In order to select proper correction models in the study area for the dry tropospheric correction (DTC), wet tropospheric correction (WTC), geocentric ocean tide correction and mean sea surface (MSS), we considered the SLA corrected by different models. The difference of SLA variances between test and reference correction models was computed as a function of distance to the coast (Fig. 1) using 84 cycles of Jason-3 data over the period of 2016–2018. In Fig. 1, the negative value of the test vs reference models indicates that the test correction model achieves smaller SLA variance than the reference model and should be selected.

The DTC handles the path delay due to dry natural gases in the atmosphere, which is usually derived from the numerical weather models such as the ECMWF (European Centre for Medium-range Weather Forecasts) operational model or the ERA (ECMWF reanalysis) model. This correction is the largest range correction with an accuracy better than 1 cm globally, but it degrades significantly in steep coastal areas where the elevation of land ranges from 500 m to 1000 m (Cipollini et al., 2017a). Here we compared the DTC from these two models. As shown in Fig. 1a, the DTC from the ERA model is comparable to that from the ECMWF operational model until 5 km to the coast, where the ERA-derived DTC has lower SLA variance.

The on-satellite microwave radiometer (MWR) derived WTC degrades in coastal areas due to land contamination. Therefore, the value from the ECMWF operational model or the ERA model is used instead. However, the 6-h temporal resolution of numerical weather models is not short enough to accurately capture the variability of WTC in coastal areas (Andersen and Scharroo, 2011). To overcome this problem, dedicated approaches were proposed to recompute the WTC (Desportes et al., 2009; Fernandes and Lázaro, 2016; Mercier et al., 2012; Obligis

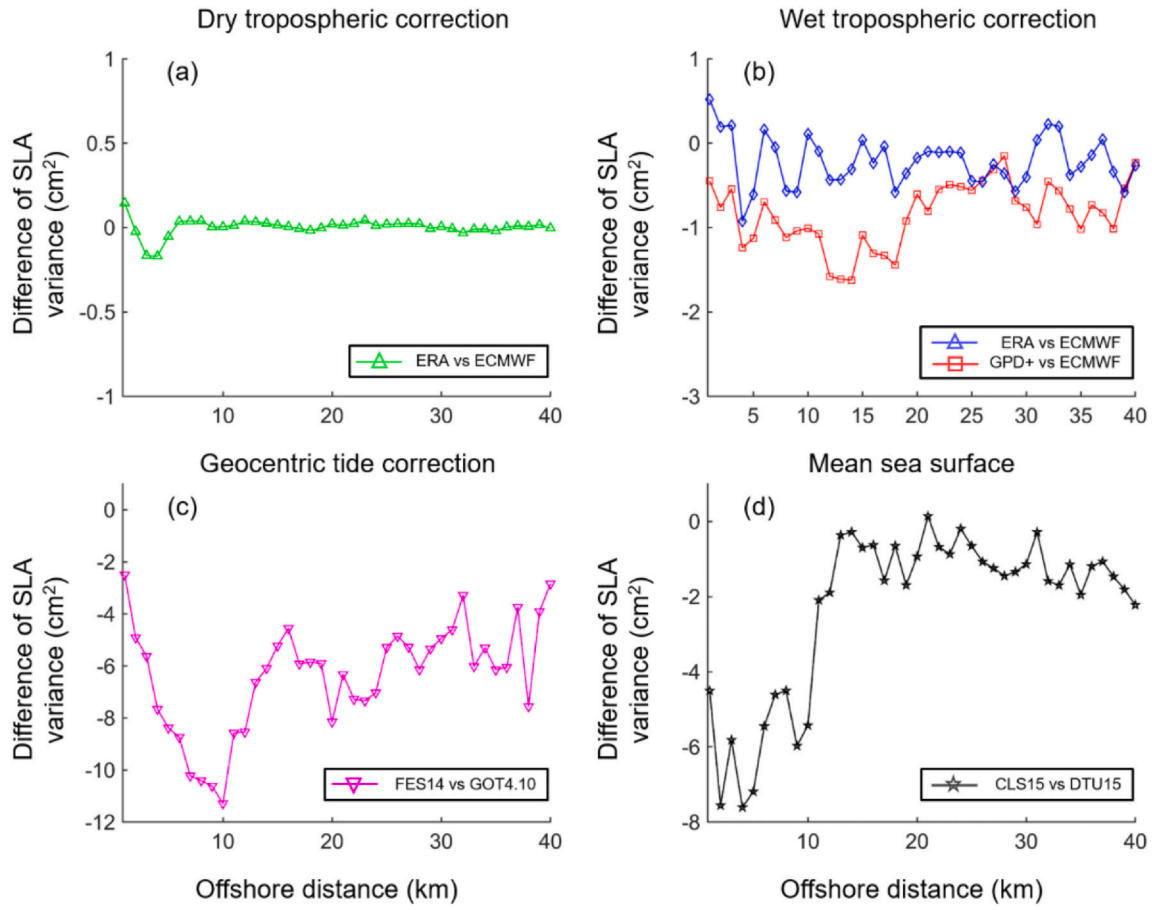

Fig. 1. Difference of SLA variances between different models (i.e. test minus reference) as a function of distance to the coast using Jason-3 data over the period of 2016–2018, with negative values indicating that the test model provides proper corrections for the study area. The results are shown for (a) DTC, (b) WTC, (c) geocentric tide correction and (d) MSS.

Table 1
Corrections and MSS used for calculating SLA estimates for Jason and Sentinel-3A altimeters.

Satellite	Jason-1	Jason-2	Jason-3	Sentinel-3A
Correction				
Dry tropospheric correction	ERA	ERA	ERA	ERA
Wet tropospheric correction	GPD+	GPD+	GPD+	ECMWF
Ionospheric correction	GIM	GIM	GIM	GIM
Dynamic atmospheric correction	MOG2D	MOG2D	MOG2D	MOG2D
Sea state bias	CLS 2012	CLS 2012	CLS 2012	CLS 2012
Geocentric tide correction	FES2014	FES2014	FES2014	FES2014
Solid earth tide	Cartwright and Taylor (1971); Cartwright and Edden (1973)	Cartwright and Taylor (1971); Cartwright and Edden (1973)	Cartwright and Taylor (1971); Cartwright and Edden (1973)	Cartwright and Taylor (1971); Cartwright and Edden (1973)
Pole tide	Wahr (1985)	Wahr (1985)	Wahr (1985)	Wahr (1985)
Mean sea surface	CLS15	CLS15	CLS15	CLS15

et al., 2011). Among them, the Global Navigation Satellite System (GNSS) derived Path Delay Plus (GPD+) algorithm combines valid measurements from MWR, GNSS coastal and inland stations, and scanning imaging MWR to improve both precision and availability of WTC (Fernandes and Lázaro, 2016), which has been used in Sea Level Climate Change Initiative project conducted by European Space Agency (Ablain et al., 2015). Fig. 1b shows the comparison of WTC from the ECMWF operational model, the ERA model and the GPD+ method. The result illustrates that the WTC derived from the GPD+ method archives the best performance over the entire 0–40 km coastal strip.

The geocentric ocean tide correction accounts for the largest ocean variability, whose performance in coastal areas is improved thanks to the continuous progress of global ocean tide models (Stammer et al., 2014). However, there still exist significant differences between different global ocean tide models in certain coastal areas, which encourages the development of regional tide models. Fig. 1c shows the result of two global ocean tide models - the Finite Element Solution 2014 (FES2014) and Goddard Ocean Tide 4.10 (GOT4.10) models. As illustrated in Fig. 1c, the FES2014 model shows better performance than the GOT4.10 model especially in the last 15 km to the coast.

The MSS is the temporal-averaged sea surface height, whose accuracy is affected by the length of averaging period, smoothing error and interpolation error (Andersen and Rio, 2011). Therefore, the MSS derived from current grid MSS models shows significant discrepancy in

coastal areas especially on uncharted ground tracks (e.g., Sentinel-3A) or over rugged bathymetry (Pujol et al., 2018). The Collecte Localisation Satellites 2015 (CLS15) and Danmarks Tekniske Universitet 2015 (DTU15) MSS models are assessed in this study. Fig. 1d illustrates that the CLS15 MSS model achieves significant improvement in the 0–15 km distance band with a variance reduction of 4–8 cm^2.

To summarize, the corrections and MSS used for calculating the SLA estimates for both Jason and Sentinel-3A altimeters are listed in Table 1. The DTC derived from ERA model, SSB correction obtained from CLS2012 non-parametric model and geocentric ocean tide correction computed from FES2014 global tide model are provided by the Radar Altimeter Database System (RADS) (Scharroo et al., 2013). The WTC derived from the GPD+ algorithm can be downloaded from https://www.fc.up.pt/Satellite_Altimetry/Wet_Tropo/GPD+/v1.0/. The dynamic atmospheric correction was calculated from the MOG2D (Modèle aux Ondes de Gravité – two dimensions) model with 1/4° × 1/4° spatial resolution and 6-h temporal resolution, which is available from ftp-access.aviso.altimetry.fr. Other corrections are contained in the Jason and Sentinel-3A official products. The GPD+ WTC is currently not available for the Sentinel-3A altimeter, so the value from the ECMWF operational model is used instead. The MSS was derived from the state-of-the-art CLS15 MSS model (Schaeffer et al., 2016).

The 20-Hz altimeter SLA estimates without SSB correction were derived following the method described in Peng and Deng (2020). The SLA estimates outside the range of [−0.5 m, +0.5 m] are considered as outliers and are removed in this study.

2.2. Study region

The Australian coastal region (10–45°S, 110–115°E) is selected in this study (Fig. 2) because of its complex coastal environment. It has a 34,000 km length of coastline and encompasses tropical, sub- and extra-tropical climates (McInnes et al., 2016), which is of high interest for oceanographic and climate studies (Deng et al., 2011). For example, the existence of coral reefs (e.g., Great Barrie Reef in Northeast and Ningaloo Reef in Northwest) results in errors in altimeter sea-level measurements as well as large variation in the coastal bathymetry, and thus making it difficult to accurately model the tidal signals (Seifi et al., 2019). In this regard, the retracked high-rate SLA datasets with a cm level precision will provide valuable inputs for oceanic applications in coastal and nearshore oceans.

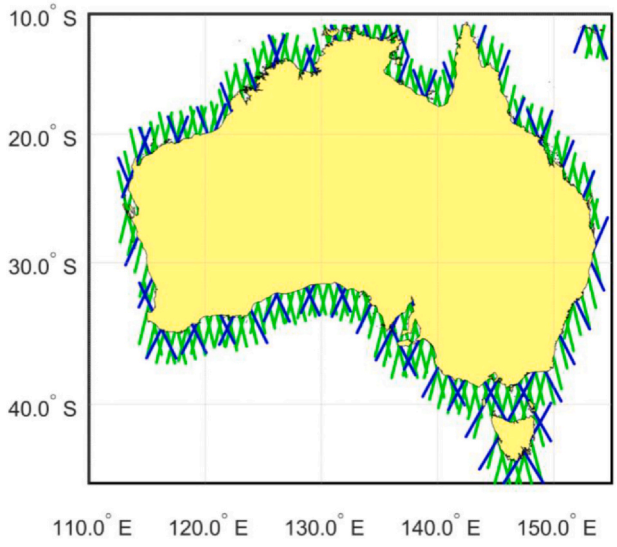

Fig. 2. Study region and the distribution of altimeter ground tracks of Jason (in blue) and Sentinel-3A (in green). Only ground track points within 100 km from the coast are used in this study. (For interpretation of the references to colour in this figure legend, the reader is referred to the web version of this article.)

3. Methodology

3.1. Estimation of intra-1-Hz correction

The intra-1-Hz correction was developed to remove the high-frequency noise caused by the correlated error between 20-Hz SLA and SWH estimates. It is applied to the SLA, which is computed following the method described by Quartly et al. (2019) as,

$$corrected\ SLA = SLA - \beta SWH \tag{1}$$

where β is a constant multiplied with SWH to derive the intra-1-Hz correction (i.e. the 2nd term in the right-hand side of Eq. (1)), which is calculated through linear regression as,

$$SLA = \beta SWH + c \tag{2}$$

where β and c are the regression slope and intercept of the fitted line between 20-Hz SLA and SWH estimates within a 1-Hz block (i.e. a vector that contains 20-Hz estimates). Because the regression slope β varies with different 1-Hz blocks, the median value of regression slopes is used to simplify the calculation (Quartly et al., 2019). To evaluate the performance of the linear model, the correlation coefficient R and coefficient of determination r^2 are also calculated as follows,

$$R = \frac{\sum_{i=1}^{n}(x_i - \bar{x})(y_i - \bar{y})}{\sqrt{\sum_{i=1}^{n}(x_i - \bar{x})^2}\sqrt{\sum_{i=1}^{n}(y_i - \bar{y})^2}} \tag{3}$$

$$r^2 = 1 - \frac{\sum_{i=1}^{n}(y_i - \hat{y}_i)^2}{\sum_{i=1}^{n}(y_i - \bar{y}_i)^2} \tag{4}$$

where x_i represents the SLA, y_i represents the SWH, n is the number of estimates in a single 1-Hz block, the over bar represents the mean value, and the hat represents the estimated value from the linear model. The r^2 is used to evaluate the goodness of fit of a linear model.

3.2. Estimation of SSB corrections

To compare the performance of SSB models, we used three sets of SSB corrections in this study. The first is the 1-Hz SSB correction derived from the CLS2012 non-parametric model (Tran et al., 2012), which is provided by the RADS product.

The second is the 20-Hz SSB correction derived from a regional parametric model using 20-Hz SLA, SWH and wind speed estimates (Passaro et al., 2018). Applying this SSB model at the 20-Hz data is capable of reducing not only the impact of local sea states, but also the correlated error between SLA and SWH estimates at the short wavelength (< 50 km). Passaro et al. (2018) recomputed the 20-Hz SSB correction based on the regional parametric model (i.e. the Fu and Glazman (1991) model). When compared to the 1-Hz SSB correction, their regional SSB model improves the precision of high-rate SLA data by ~30% in the Mediterranean Sea and North Sea (Passaro et al., 2018). The approach taken in this paper is similar to that taken by Passaro et al. (2018), except for that we used the BM4 model (Gaspar et al., 1994) described in Eq. (5) as the regional parametric model for Australian coastal zones.

The third is the composite SSB correction proposed in this study, which is derived in three steps. Firstly, the intra-1-Hz correction was computed using the method described in Section 3.1 and applied to the 20-Hz SLA estimates accordingly to reduce the high-frequency SLA noise. Secondly, the regional BM4 model (i.e. Eq. (5)) was built to generate 1-Hz SSB correction using 1-Hz SLA, SWH and wind speed estimates derived from corresponding 20-Hz estimates. Finally, in order to correct 20-Hz SLA estimates, the 1-Hz SSB correction was interpolated to 20-Hz SSB correction using the nearest neighbourhood approach. Here, applying the intra-1-Hz correction to the 20-Hz retracked SLA removes the high-frequency error caused by correlation between SLA and SWH. The recomputed 1-Hz SSB correction is thus only related

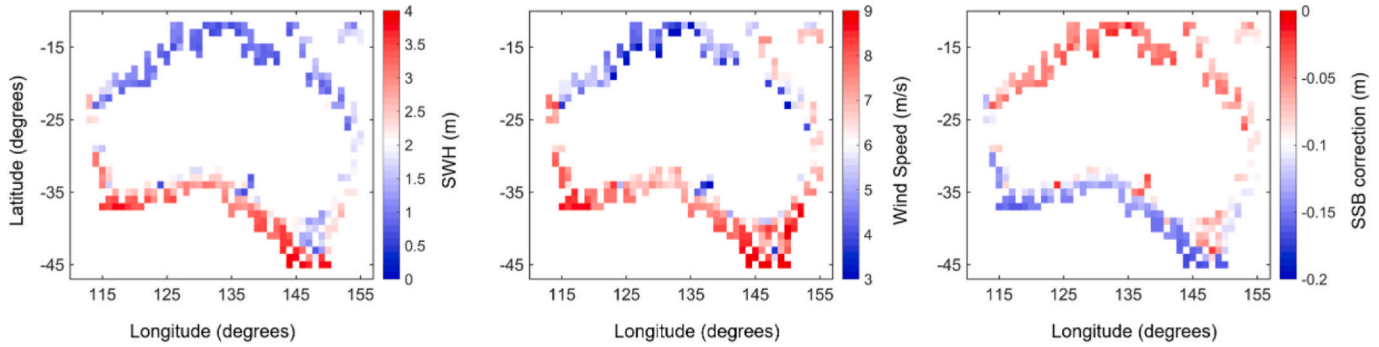

Fig. 3. Mean value of 20-Hz SWH (left), wind speed (middle) and composite SSB correction (right) estimates computed on 1-degree grids for MBP-retracked Jason-3 over the period of 2016–2018.

to the regional sea state effects. In this way, we estimate the regional SSB correction using the SLA free from the correlated error.

The BM4 model described in Gaspar et al. (1994) is as follows,

$$SSB = SWH\,[a_1 + a_2 SWH + a_3 U + a_4 U^2] \tag{5}$$

where U is the altimeter wind speed computed from the sigma0 estimated by retrackers (e.g., MBP and SAMOSA+) using Abdalla's model (Abdalla, 2012), a_1, a_2, a_3 and a_4 are four parameters of the model. These four parameters can be estimated through,

$$\Delta SLA_i = \Delta SSB_i + \varepsilon_i \tag{6}$$

where ΔSLA_i is the SLA difference between ascending and descending tracks at the i^{th} crossover point, ΔSSB_i is the SSB difference between ascending and descending tracks at the i^{th} crossover point, ε_i is the residual that cannot be explained by the SSB correction. The ordinary least squares estimator is used to solve Eq. (6), obtaining the value and uncertainty of the four unknown coefficients. Since the quality of altimeter data degrades near the coast, only crossover points beyond 20 km from the coast are used to guarantee the robustness of the empirical model. To make a trade-off between reducing the impact of oceanic variability and retrieving enough crossover points, we only consider crossover points with temporal differences shorter than 10 days.

The BM4 parametric model rather than non-parametric model is used in this study for two reasons. First, the parametric model is easy to conduct and computationally efficient. Second, the performance of regional parametric model on reducing the SLA noise has been proved (Passaro et al., 2018). Note that the 1-Hz SSB correction from the CLS2012 non-parametric model for Jason altimeters (Table 1) is dependent to the SGDR MLE4 retracker but not the MBP retracker used in this study. Therefore, the SLA without SSB correction is taken as the reference to evaluate the performance of above three sets of SSB corrections.

3.3. Methods for precision analysis

In order to analyze the data precision, we used two statistical parameters to first assess the extent of noise reduction by adding SSB corrections introduced in Section 3.2, and then to quantify the noise level of 20-Hz SLA estimates. Theses parameters are the percentage of noise reduction (PNR) and high-rate SLA noise.

The PNR is used to assess the improvement of SLA precision, which is based on the variance of SLA estimates on a 1° × 1° grid. This metric is commonly used to examine the performance of corrections on SLA estimates (e.g., Carrère and Lyard, 2003; Fernandes et al., 2015; Pascual et al., 2008; Passaro et al., 2018; Tran et al., 2010a). The PNR on each 1-degree grid is calculated as,

$$\mathrm{PNR} = \frac{Var(SLA1) - Var(SLA2)}{Var(SLA1)} \times 100 \tag{7}$$

where SLA1 and SLA2 represent the SLA without and with the selected correction, respectively. *Var(SLA)* is the variance of all SLA estimates falling into a 1-degree grid over the period of a single mission. In this study, the 1-Hz, 20-Hz and composite SSB corrections are to be tested. According to Eq. (7), the positive PNR indicates that the precision of SLA is improved after applying the selected correction. The overall improvement in the study area is represented as the median value of PNR parameters on all 1-degree grids.

The high-rate SLA noise was evaluated as the absolute differences between two consecutive along-track SLA estimates. This method was proposed by assuming that SLA estimates are not significantly changed at the spatial scales (i.e. 300–350 m along-track) of 20-Hz altimeter measurements (Cipollini et al., 2017b; Passaro et al., 2014; Passaro et al., 2018). To clearly illustrate the relation between SLA noise and offshore distance, the high-rate SLA noise is computed on a 1 × 1 km grid according to the offshore distance in the along-track and across-track directions. The median value of each grid was computed, because it is a good indicator to evaluate the noise level (Cipollini et al., 2017b).

4. Results and discussion

The composite SSB correction differs from the 20-Hz SSB correction, because it separately treats the correlated error between SLA and SWH estimates, and SSB related to the sea states. Therefore, we first illustrate the intra-1-Hz correction, followed by the 20-Hz and composite SSB corrections.

4.1. Intra-1-Hz correction

Since the intra-1-Hz correction was developed to depict the correlated error between SWH and SLA estimates, it can be simply modelled using a linear relationship determined by the regression slope (Quartly et al., 2019). Fig. 3 shows the distribution of estimated regression slopes of β (cf. Eq. (2)) obtained from all 1-Hz blocks for MBP-retracked datasets of Jason-1/2/3 and SAMOSA+ retracked dataset of Sentinel-3A. Each median value of β was used to calculate the intra-1-Hz correction to the retracked 20-Hz measurements from the corresponding altimeter. The two measures of the regression model, R and r^2, are also shown in Table 2.

As illustrated in Table 2, the 20-Hz SLA estimates are negatively correlated with SWH estimates. The median values are almost the same around −0.087 though the lengths of data are about seven, eleven and two years for Jason-1, Jason-2 and Jason3, respectively. This result demonstrates that the regression slope is significantly dependent on the combination of the altimeter and retrackers. Because the Jason missions have the same work principles, the regression slope β is therefore primarily determined by the MBP retracker. The value of our β estimates (around −0.087) from SLA data for Jason missions is similar to that (−0.102) for β estimated from an analysis by Quartly et al. (2019) using 10 cycles of Jason-3 MLE4 retracked raw SSHs.

Table 2 also reveals that Sentinel-3A's regression slope shows a

Table 2
The median value of regression slope β used to calculate the intra-1-Hz correction for four altimeters (i.e. Jason-1/2/3 and Sentinel-3A). The retrackers used are the MBP for Jason 20-Hz data and SAMOSA+ for Sentinel-3A 20-Hz data. The R is the correlation coefficient, while r^2 is the coefficient of determination.

Altimeters	Number of 1-Hz block	Median β	Median R	Median r^2
Jason-1	362,196	−0.085	−0.52	0.32
Jason-2	442,348	−0.087	−0.53	0.33
Jason-3	241,435	−0.087	−0.51	0.31
Sentinel-3A	182,717	−0.046	−0.28	0.13

different pattern from Jason missions. This is expected because Sentinel-3A adopts the Delay-Doppler technique, and thus the trailing edge of the SAR waveform decays much faster than the pulse-limited waveform (Dinardo et al., 2018; Ray et al., 2014). The low correlation coefficient (−0.28) for Sentinel-3A SAMOSA+ retracker indicates that the 20-Hz SLA estimates have a weak linear relationship with SWH estimates in the SAR mode.

The coefficients of determination r^2 are small for all altimeters, indicating that the linear model (Eq. (2)) can only explain a small portion of variance in SLA estimates. However, the correlation coefficient R around −0.52 for Jason missions suggests that there is a moderate negative correlation between SLA and SWH estimates. In addition, the regression slope β shows good performance by reducing the correlated error (Quartly et al., 2019).

From the above analysis, there exists a negative correlation between the SLA and SWH for Jason missions in the study area, leading to the non-zero regression slope β. Therefore, applying the intra-1-Hz correction (Eq. (1)) is necessary to reduce the correlated error between SWH and SLA estimates.

4.2. SSB correction

Tables 3 and 4 show the coefficients of BM4 model for each altimeter used to generate 20-Hz and composite SSB corrections, respectively. According to the results presented in both tables, each altimeter has a different set of coefficients. After removing the high-frequency noise caused by the correlated error between SLA and SWH estimates, the coefficients become more consistent for Jason altimeters (Table 4). This suggests that the removal of retracker-induced correlated error contribute to the unification of SSB models, because the EM bias and skewness bias are theoretically the same for all conventional Ku-band altimeters (Gaspar et al., 1994; Passaro et al., 2018; Quartly et al., 2019).

Fig. 3 shows the mean value of 20-Hz SWH, wind speed estimates and composite SSB correction computed on 1-degree grids for MBP-retracked Jason-3. As shown in Fig. 3, the sea states in the northern part of Australia show different patterns from other parts of Australia, with SWH and wind speed estimates being smaller than ~1.5 m and ~6 m/s, respectively. To the south of Australia, the means of SWH and wind speed estimates gradually increase up to 4 m and 9 m/s, respectively. This is because the sea states in the northern part of Australia are affected by the monsoon and trade winds, while increased wave heights in the South Australia are due to the westerly winds and Southern Ocean Swell (Hemer et al., 2007). As a result, the composite SSB correction has larger magnitude in the South Australia than that in the northern part of Australia, with the value ranging between −0.2 m and 0.0 m.

Table 3
Coefficients of BM4 model (Eq. (5)) built with 20-Hz altimeter SLA, SWH and wind speed estimates before adding the intra-1-Hz correction.

Altimeters	a1	a2 (m^{-1})	a3 $(m/s)^{-1}$	a4 $(m/s^{-2})^{-1}$
Jason-1	−0.0200	−0.0106	0.0027	−9.4858e-5
Jason-2	−0.0625	−0.0032	0.0020	−2.9360e-5
Jason-3	−0.0966	0.0029	0.0035	−1.0341e-4
Sentinel-3A	−0.0381	−5.7852e-4	−7.7977e-4	2.7405e−5

Table 4
Coefficients of BM4 model (Eq. (5)) built with 1-Hz altimeter SLAs, SWHs and wind speeds after adding the intra−1-Hz correction.

Altimeters	a1	a2 (m^{-1})	a3 $(m/s)^{-1}$	a4 $(m/s)^{-2}$
Jason-1	0.0317	0.0038	−5.1437e-4	−1.7994e-5
Jason-2	0.0398	0.0023	−0.0014	−5.9748e-5
Jason-3	0.0347	0.0034	−7.2210e-4	2.6271e-5
Sentinel-3A	0.0068	0.0039	−0.0027	9.3622e-5

4.3. Precision analysis

In this section, we analysed the precision of retracked SLA estimates adjusted by three sets of SSB corrections in the Australian coastal zone. First, we checked the data availability for different altimeters after removing the SLA outliers. Second, the percentage of noise reduction due to applying 1-Hz, 20-Hz and composite SSB corrections were analysed and presented. Finally, the precision of SLA estimates in the last 40 km to the coast was investigated.

4.3.1. Data availability

Fig. 4 shows the data availability computed on a 1 × 1 km grid depending on the along-track and across-track distances of 0–40 km from the coast. To guarantee the robustness of the result, the grids where the number of measurements is smaller than 30 are displayed as white pixels. As shown in Fig. 4, the SAMOSA+ retracked Sentinel-3A achieves the highest data availability, followed by the MBP-retracked Jason-3 and Jason-2. The MBP-retracked Jason-1 shows the lowest data availability, with the percentage decreasing to only 60%–70% in the last 10 km off the coast. The degradation of Sentinel-3A is mainly observed within 5 km to the coast in the across-track direction, where the percentage varies between 50% and 70%. Compared to Sentinel-3A, the data availability of Jason missions is affected by contamination from both along-track and across-track directions, with lower data availability (40% ~ 60%) observed in the along-track direction within 5 km to the coast.

This result is expected considering the different shapes of footprint between these two types of altimeters. The Jason missions have pulse-limited altimeters, with the footprint being a circle, therefore, the contamination from different directions would equally affect the data quality. The Sentinel-3A, however, is operated in SAR mode, whose footprint is a rectangle with the across-track dimension much longer than the along-track dimension. As a result, it can better avoid the contamination from the along-track direction.

4.3.2. Improvement by SSB corrections

In order to quantify the improvement brought by different sets of SSB corrections, the metric PNR introduced in Section 3.3 is used. Fig. 5 shows the PNR values computed on 1-degree grids around the Australian coastal zone for Jason-3 and Sentinel-3A. From top to bottom, the graph shows the PNR with the 1-Hz, 20-Hz and composite SSB corrections with respect to the SLA dataset without SSB correction. Since the 1-Hz SSB correction dedicated to the MBP retracker is currently not available, we use the SGDR MLE4 SLA estimates to evaluate the performance of 1-Hz SSB correction for Jason altimeters. The results for Jason-1 and Jason-2 are not shown but listed in Table 4 due to their similarity to that of Jason-3.

According to the results shown in Fig. 5, the positive PNR values indicates that applying the 1-Hz, 20-Hz and composite SSB corrections can reduce the SLA noise in these areas, while the negative PNR values

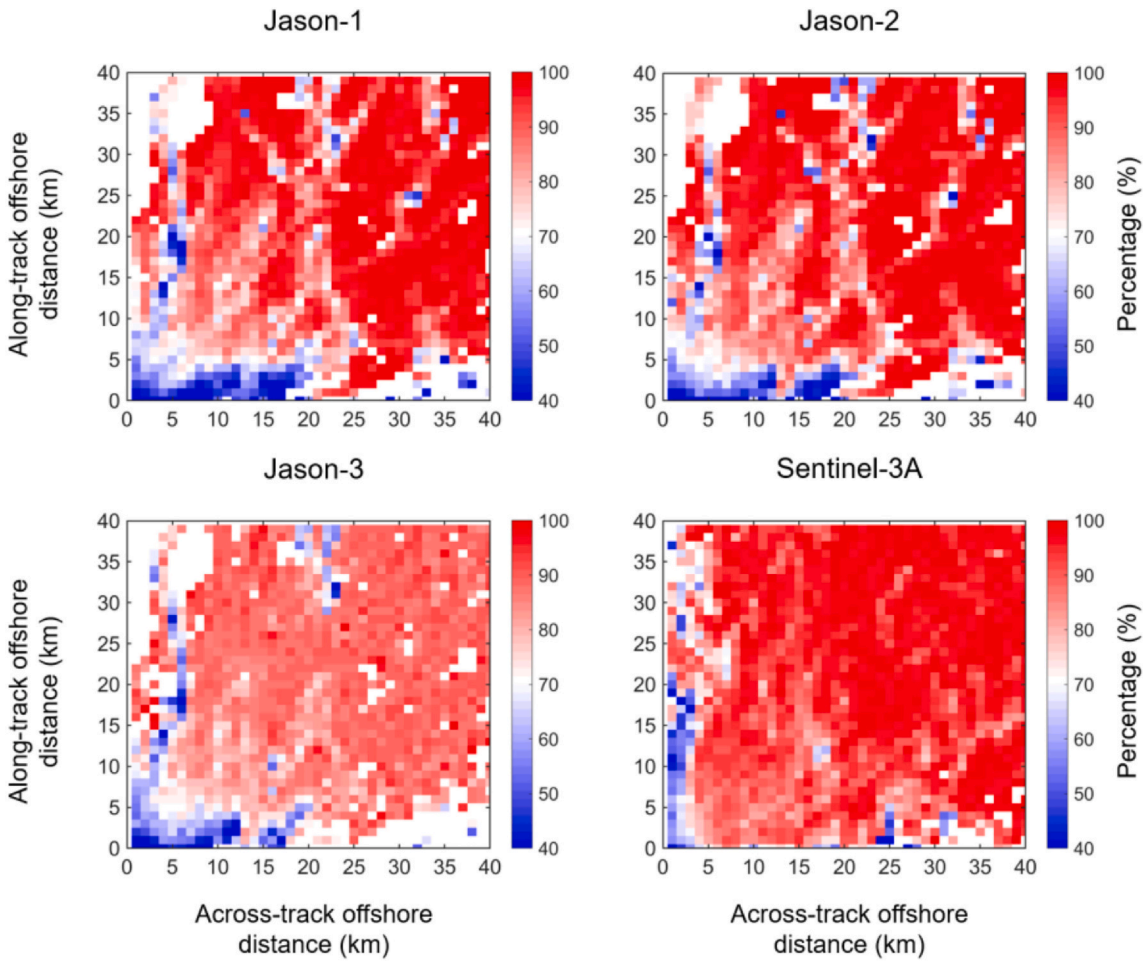

Fig. 4. Data availability for different altimeters computed on 1 km × 1 km grids depending on the offshore distance in the along-track (y-axis) and across-track (x-axis) directions. White pixels indicate there are no data available.

distributed along the Australia coast zone implies that the SSB corrections are incorrectly modelled in these regions.

For Jason-3, it can be seen that the best performance belongs to the composite SSB correction, followed by 20-Hz and 1-Hz SSB corrections. This is especially true in the Spencer Gulf (34°17′S, 136°58′E) along the south coast of Australia, where negative PNR values appear for the 1-Hz and 20-Hz SSB corrections. However, the positive PNR values for the composite SSB correction at the same place reduce the SLA variances by about 10%. Both 20-Hz and composite SSB corrections have superior performance to 1-Hz SSB correction, indicating that the 1-Hz SSB correction cannot remove high-frequency noise induced by the correlated error between SLA and SWH estimates.

It is interesting to find in this study that the performance of selected SSB corrections (i.e. 1-Hz, 20-Hz and composite SSB corrections) degrades significantly for Sentinel-3A as we can see many negative PNR values along the coast in Fig. 5. This may be explained by two reasons. First, the correlation between SWH and SLA is low (−0.28) as shown in Table 2, and thus the precision of SAR model SLA estimates is less affected by the intra-1-Hz covariant error. Second, the along-track footprint size (~300 m against a few km in conventional altimetry of Jason missions) is smaller than some of long ocean waves, and thus only covers a portion of the long ocean waves (Moreau et al., 2018). As a result, both the non-parametric and empirical parametric SSB models developed for conventional altimeters and used in this study are not adaptive to the SAR mode altimeter. Therefore, it is vital to develop a dedicated model or parametrization of the SSB for the SAR mode altimeter in the future.

To summarize the results, the median value of all PNR values was calculated and displayed in Table 5. For Jason missions when compared to high-rate SLAs without SSB corrections, the improvement brought by the 20-Hz SSB correction varies between 8% and 11%, while the PNR by the composite SSB correction achieves a higher level from 12% to 14%. Both 20-Hz and composite SSB corrections have an insignificant impact on Sentinel-3A, with the percentage being 4% and 3%, respectively.

4.3.3. Precision of SLA estimates

As described in Section 3.3, the absolute differences between consecutive SLA estimates are calculated on a 1 × 1 km grid according to the offshore distance in the along-track and across-track directions. The median value of all absolute differences in each grid is used to indicate the noise level of 20-Hz SLA estimates. Fig. 6 shows the noise level of 20-Hz SLA estimates from MBP-retracked Jason-3 and SAMOSA+ retracked Sentinel-3A. From top to bottom in Fig. 6, the noise levels of 20-Hz SLA estimates without SSB correction, with 20-Hz SSB correction and with composite SSB correction are shown, respectively. The white pixels indicate there are no data available.

The results show that the application of both 20-Hz and composite SSB corrections can significantly improve the precision of 20-Hz SLA estimates for Jason-3. Beyond 10 km from the coast, the noise level decreases from ~7 cm to ~5 cm, with the colour changing from light blue to dark blue. However, the improvement for Sentinel-3A in the same distance band is negligible (right panels in Fig. 6), which is consistent with the results in Fig. 5. Within 10 km from the coast, the noise reduction for Jason missions is even more significant, with the noise level declining by a factor of 33% from ~9 cm to ~6 cm. As a result, the

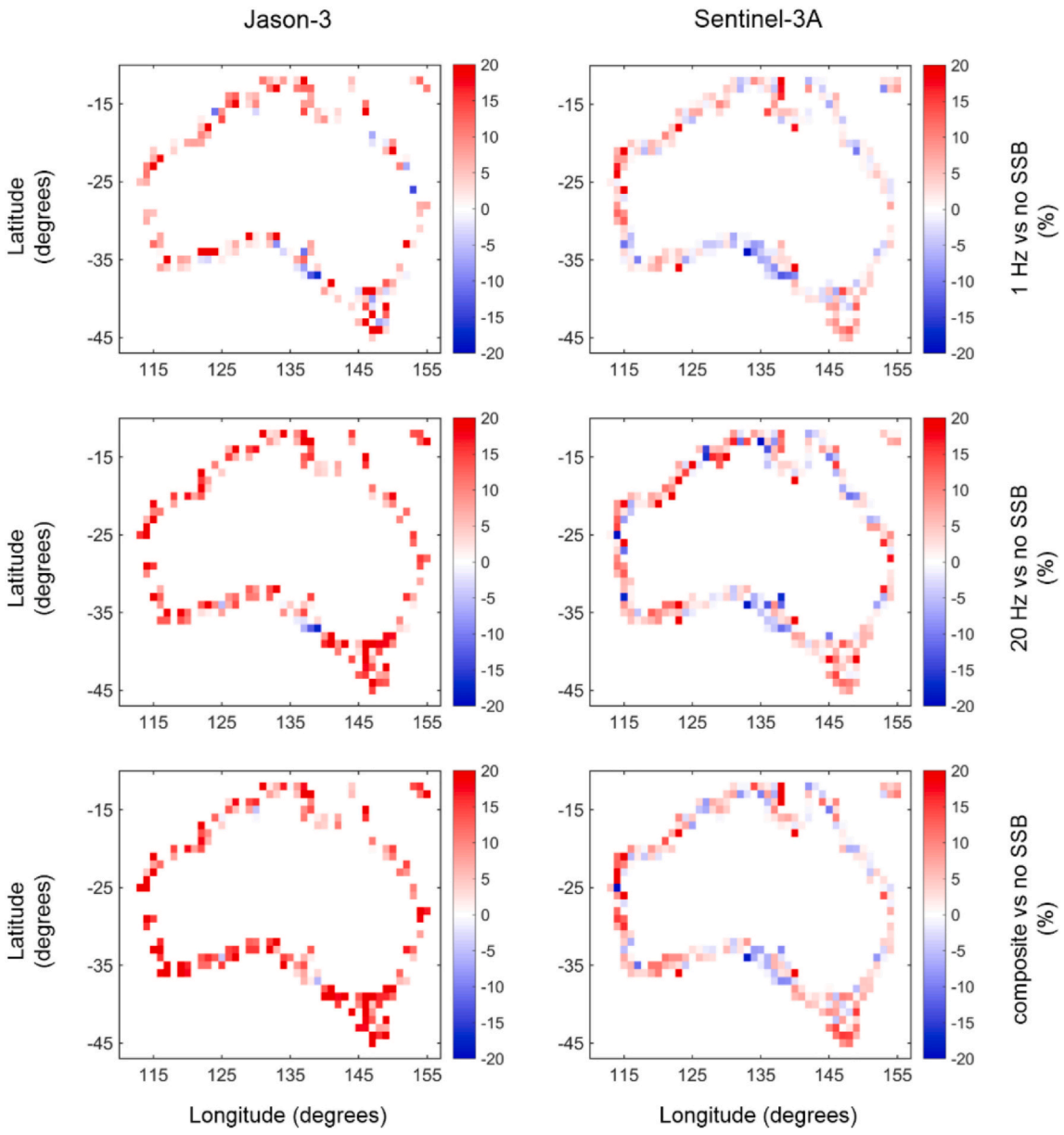

Fig. 5. Percentage of noise reduction brought by different SSB corrections for Jason-3 (left panel) and Sentinel-3A (right panel) using data within 100 km from the Australian coast. From top to bottom, the graph shows the results for 1-Hz, 20-Hz and composite SSB corrections with respect to the SLA dataset without SSB correction. Since the 1-Hz SSB correction dedicated to the MBP retracker is currently not available, we use the SGDR MLE4 retracked SLA estimates to evaluate the performance of 1-Hz SSB correction for Jason altimeters.

Table 5
Percentage of noise reduction brought by different SSB corrections for different altimeters in Australian coastal zones.

Altimeters	1-Hz[a] vs no SSB (%)	20-Hz vs no SSB (%)	Composite vs no SSB (%)
Jason-1	2.04	8.17	13.70
Jason-2	2.39	10.76	13.18
Jason-3	1.74	10.21	12.04
Sentinel-3A	1.08	3.66	3.06

[a] Jason missions use the SGDR MLE4-retracked SLA dataset and corresponding 1-Hz SSB correction, as the 1-Hz SSB correction dedicated to the MBP retracker is currently not available.

precision of SSB-corrected SLA estimates remains at the level of 4–6 cm until 5 km to the coast.

After applying the SSB correction, the degradation of Jason missions mainly comes from the along-track direction. It is observed that the noise level increases by a factor of two from ~6 cm to ~12 cm when the along-track offshore distance decreases to less than 3 km (not shown due to limited colour range). The degradation is much smaller when the across-track offshore distance decreases to less than 3 km, because the MBP retracker can successfully reduce the contamination in the waveform trailing edge (Peng and Deng, 2018a, 2020). When looking at Sentinel-3A, the degradation from the along-track direction is insignificant, where the noise level is similar to that offshore. However, the deterioration in the last 4 km from the across-track direction is considerable, with the magnitude of SLA noise being at the level of ~12 cm. The high noise level of Sentinel-3A SLA estimates may be caused again by land returns covered within its large footprint size in the across-track direction. This suggests that further effort should be made for developing new retrackers for Sentinel-3A to deal with the contamination in the across-track direction.

To summarize the results, the mean and standard deviation of all

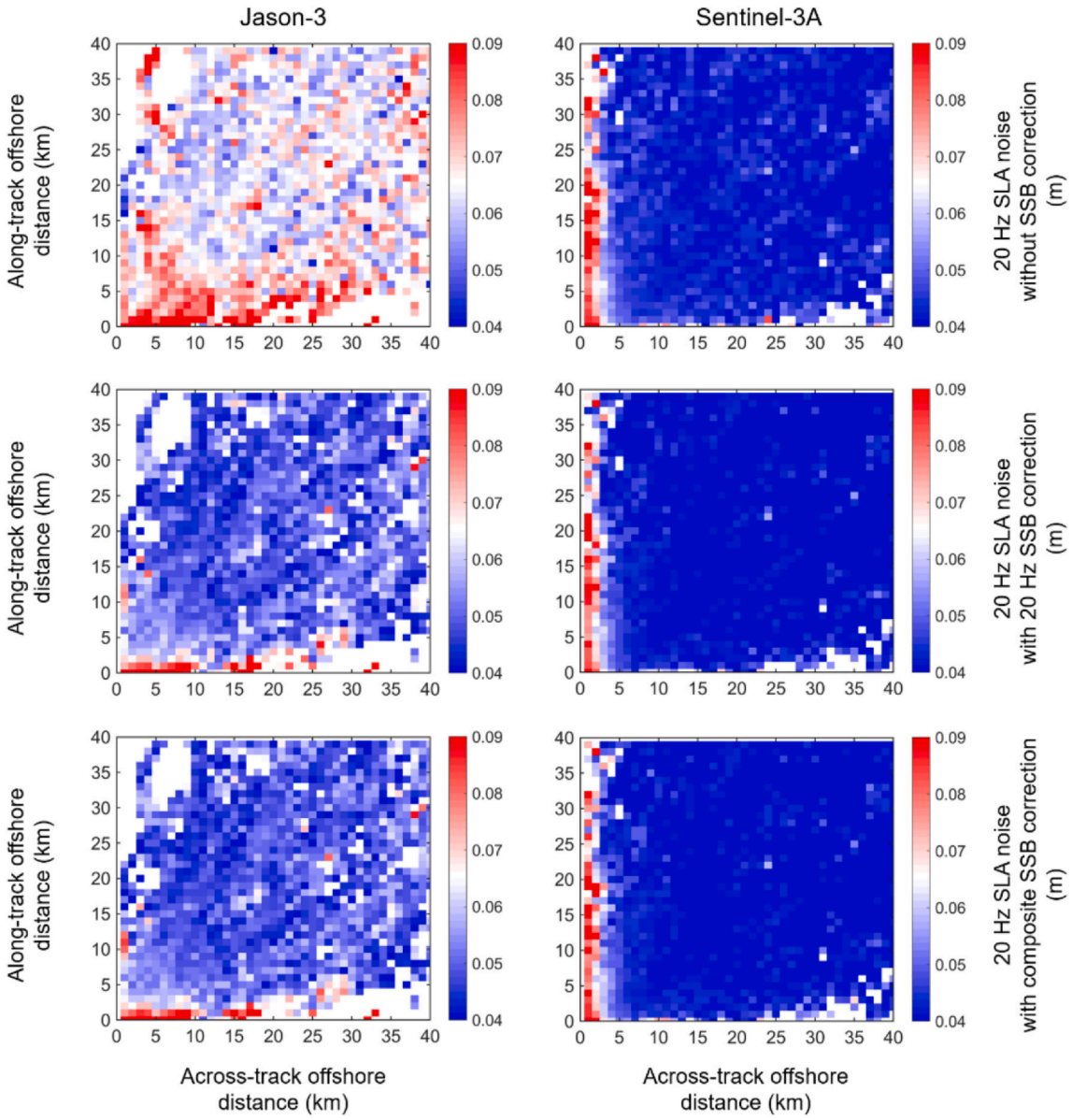

Fig. 6. Noise level of Jason-3 MBP-retracked (left panel) and SAMOSA+ retracked Sentinel-3A (right panel) 20-Hz SLA estimates. Three cases are illustrated from top to bottom of the graph: 1) 20-Hz SLA estimates without SSB correction; 2) 20-Hz SLA estimates with 20-Hz SSB correction and 3) 20-Hz SLA estimates with composite SSB correction. The noise level is computed on 1 × 1 km grids depending on the offshore distance in the along-track (y-axis) and across-track (x-axis) directions. The median value of each grid is represented as an indication of the noise level. White pixels indicates there are no data available.

Table 6
Noise level of SLA estimates without SSB, with 20-Hz SSB correction and composite SSB correction in the 0–40 km coastal strip for all altimeters in the study region.

Altimeter	No SSB (cm)	20-Hz SSB (cm)	Composite SSB (cm)
Jason-1	6.7 ± 1.1	5.6 ± 1.0	5.1 ± 1.0
Jason-2	6.7 ± 1.4	5.3 ± 1.3	5.1 ± 1.3
Jason-3	6.7 ± 1.2	5.2 ± 1.0	5.1 ± 1.0
Sentinel-3A	4.5 ± 1.0	4.2 ± 0.9	4.2 ± 0.9

absolute differences in each 1 × 1 km grid were calculated and presented in Table 6 for all altimeters. After applying the 20-Hz or composite SSB correction, the noise level (~5.2 cm) of 20-Hz SLA estimates for Jason missions is very close to that (~4.2 cm) of Sentinel-3A, with only ~1 cm difference. For Sentinel-3A, however, the noise level is currently estimated based on the SLA data corrected by the inappropriate SSB model. The development of a more appropriate SSB model for Sentinel-3A and SAR-mode datasets is again necessary in the future research.

4.4. Geographical characteristics of SLA variance

In this section, we study the data quality depending on the geographical location. The data quality is represented as the median value of SLA variances after applying the composite SSB correction computed on 1-degree grids. Fig. 7 shows the results for all four altimeters around the Australian coastal zone.

As illustrated in the graph, the SLA variance in most places along the coast varies between 0.02 m^2 and 0.04 m^2. The deterioration is observed in certain places such as the Gulf of Carpentaria and the Great Barrier Reef (Fig. 7), where the variances increase up to 0.06–0.1 m^2. In order to better illustrate the geographical features and reasons leading to the degradation of data quality, the along-track SLA estimates in

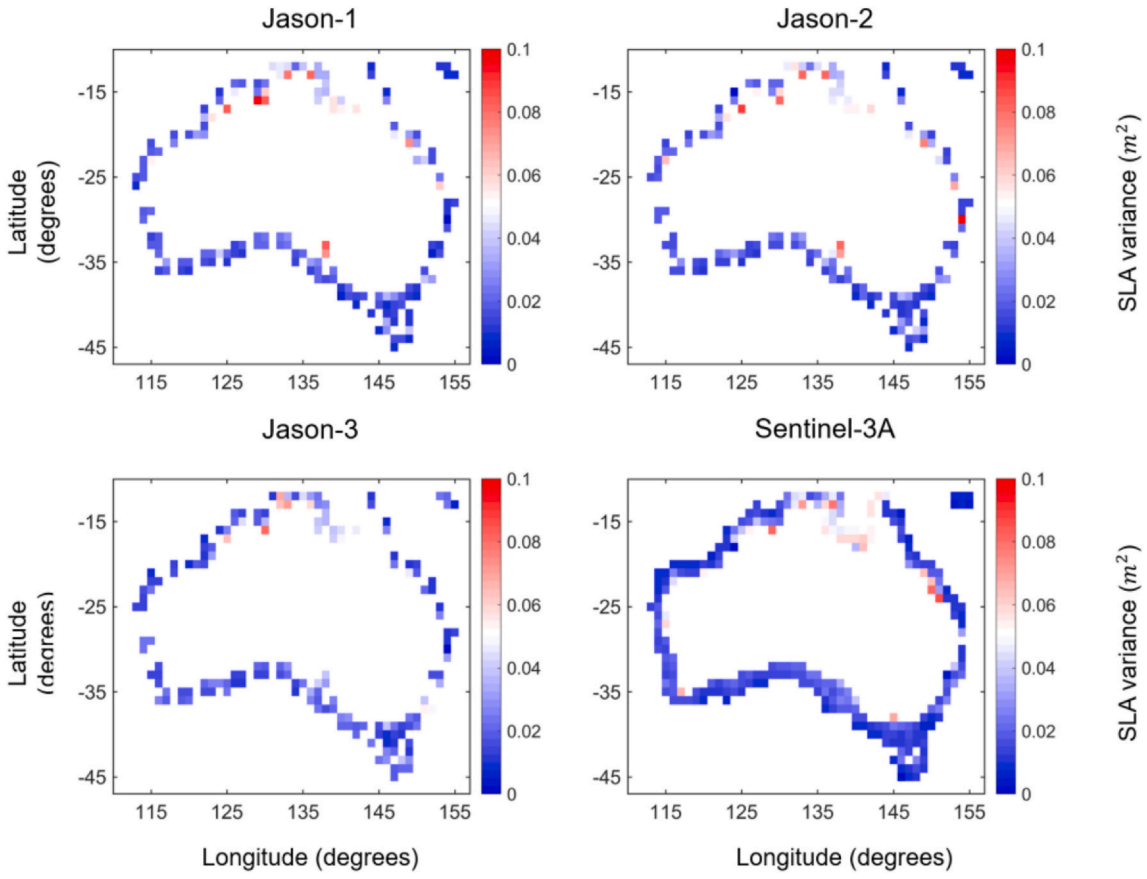

Fig. 7. SLA variances computed on 1-degree grids for all four altimeters around Australian coastal zone. The composite SSB correction has been applied to SLA estimates.

these areas are given in Fig. 8.

The first factor leading to the data degradation is the complex coastal morphology. Fig. 8a shows the SLA variation as the altimeter moves from the open ocean to the Victoria River. Because the sea surface roughness is relatively small around estuaries, the waveform becomes Quasi-specular. The MBP retracker cannot properly handle this type of waveform so far, leading to the degradation in this area. Besides, when the altimeter gets closer to the strait, multiple small islands and large island (Fig. 8b–d), the significant increase in the along-track SSH values was observed. The waveforms measured in these areas are mostly Brown-peaky waveforms with high peak amplitude, indicating that the waveforms are seriously contaminated by the land returns. As a result, the noise level of SLA within 3 km off the coast is very high as illustrated in Fig. 6.

The second reason is the degradation of geophysical corrections, especially the geocentric ocean tide correction. In the area of Great Barrier Reef (Fig. 8e) between 20°S and 24°S, the ocean tide correction from FES2014 is not accurate because the bathymetry here fluctuates significantly (Seifi et al., 2019). Seifi et al. (2019) developed a regional ocean tide model that achieves better performance than global ocean tide models in this region. We did not use this regional model because it now only covers a small portion of the Australian coastal zone. This would be greatly beneficial for improving the precision of SLA estimates once the regional tidal correction is ready for use.

Finally, the parallel orientation of the ground track with respect to the coastline would cause significant data degradation for Sentinel-3A (Fig. 8f). As shown in the graph, the flight direction is nearly parallel to the coastline, where the waveform is more likely to be contaminated due to the larger across-track dimension (~16 km) and the across-track noise level can be as high as ~0.1 m within ~3 km from the coast (Fig. 6). The Jason missions should not be affected by this orientation issue because of their circular footprint, which has the same dimension in both along-track and across-track directions. However, the footprint size of Jason missions can be as large as 20 km depending on the wave conditions (Peng and Deng, 2018b), which may cause a long distance waveform contamination in the along-track direction. The evaluation results from Fig. 6 show that the along-track contamination is more serious than the across-track contamination, indicating that the orientation of ground track also affects the performance of Jason missions.

Since the noise level of SLA estimates within 3 km to the coast is extremely high (Fig. 7), we also investigated the waveform shapes in this coastal strip to explore the potential of recovering reliable sea level data. A waveform classification was conducted for a single cycle of Jason-3 and Sentinel-3A waveform data, respectively. The waveforms were classified into different groups according to their shapes (not shown). The results demonstrate that there are still about 53% of Jason-3 and 49% of Sentinel-3A waveforms that cannot be accurately recovered in the 0–3 km coastal strip by using current retrackers in Australian coastal zones. These waveforms are seriously contaminated due to strong inhomogeneous reflections within the altimeter footprint, and therefore causing the degradation of SLA precision (and consequently incorrect SSB corrections). As such, retracked SLA data in the 0–3 km coastal strip should be used with caution.

5. Conclusions

In this study, the precision of 20-Hz SLA estimates with three sets of SSB corrections (i.e. 1-Hz, 20-Hz and composite SSB models) within 100 km to the Australian coastline was analysed using 16 years of MBP-retracked Jason-1/2/3 data and 3 years of SAMOSA+ retracked Sentinel-3A data. We focused on removing the noise from 20-Hz SLA

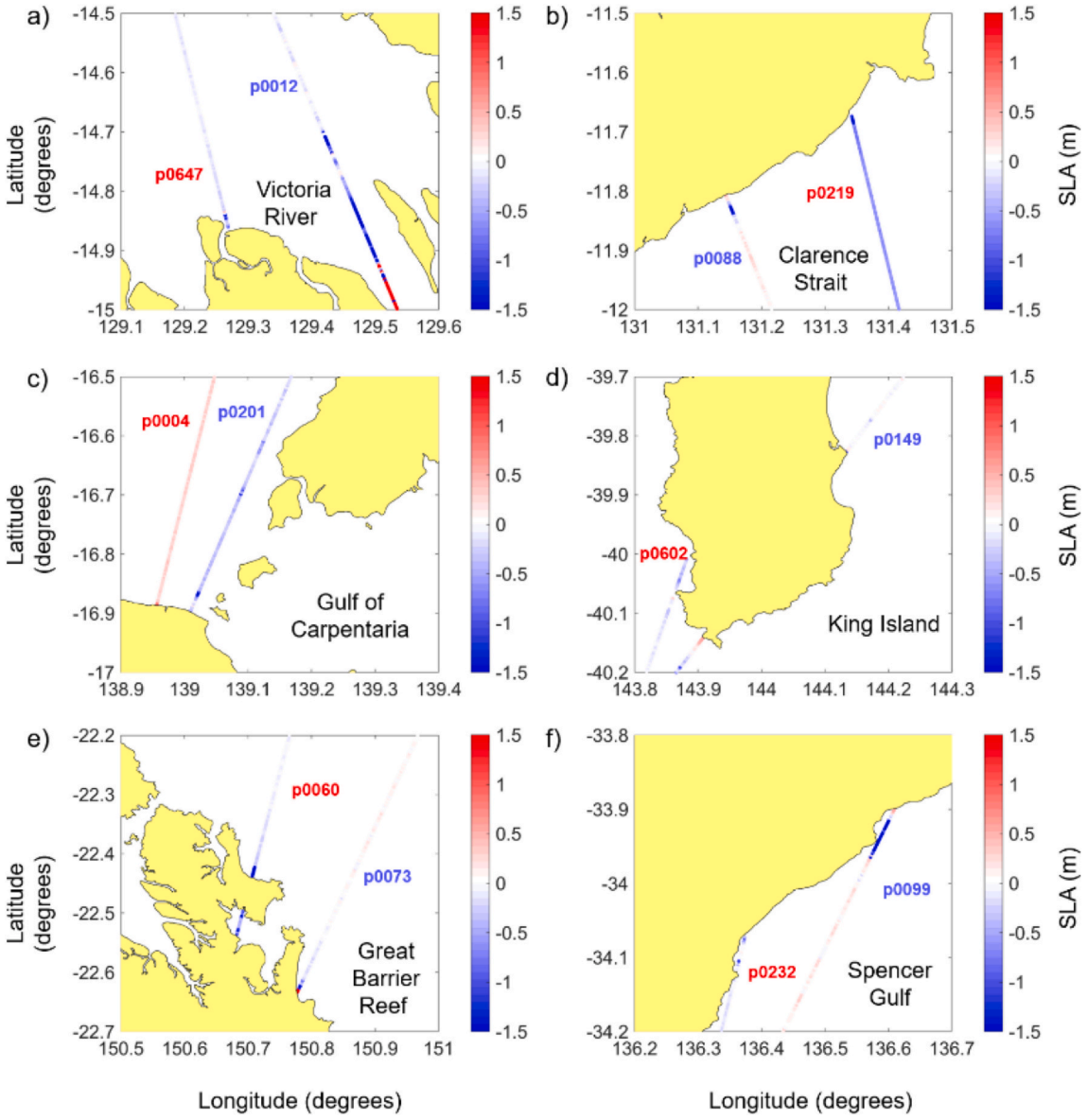

Fig. 8. Along-track SLA estimates after applying the composite SSB correction for MBP-retracked Jason-3 and SAMOSA+ retracked Sentinel-3A. The track number is presented in blue bold font for Jason-3 and in red bold font for Sentinel-3A, respectively. (For interpretation of the references to colour in this figure legend, the reader is referred to the web version of this article.)

estimates via applying the intra-1-Hz and recalculated SSB corrections. The performance of SSB corrections on reducing the SLA noise was assessed. The SLA's precision was evaluated in the 1 × 1 km grids and presented in different coastal zones.

The composite SSB correction that combines the intra-1-Hz correction and 1-Hz SSB correction is found to achieve better performance than 20-Hz SSB correction in the study region. After applying the 20-Hz and composite SSB corrections, the noise level of MBP-retracked SLA estimates is reduced on average by a factor of 10% and 13%, respectively, over the entire study area. Although a difference of 3% of noise reduction between two models may not be significant, the composite SSB correction provides at least a different method that is as effective as the 20 Hz SSB correction for high-rate SLA estimates.

Both the non-parametric and parametric SSB corrections have little impact on reducing Sentinel-3A SLA noise, with the noise reduction at the level of ~3%. Therefore, it is necessary to develop a more appropriate SSB model for the SAR mode altimeter.

The precision of SSB-corrected SLA estimates (i.e. absolute differences between two consecutive SLA estimates) keeps at the levels of ~5 cm and ~ 4 cm from the open ocean until 3 km to the coast for Jason altimeters and Sentinel-3A, respectively. The degradation of Jason missions is mainly observed in the along-track direction, while the deterioration of Sentinel-3A primarily comes from the across-track direction. Therefore, it is still important to investigate how to reduce the contamination from the across-track direction, in particular within 10 km from the coast, in order to further improve the performance of Sentinel-3A near the shore.

The reliability of retracked SLA estimates is still challenging in certain areas such as estuaries and straits, where the noise level is about 3–4 times higher than that that in other coastal areas. Since these areas are important for studying coastal sea level changes and other oceanographic processes (Durand et al., 2019; Gómez-Enri et al., 2019), it is essential to make further efforts and improve the precision of retracked data in these areas.

Author contributions

Fukai Peng conducted conceptualization, investigation, data

curation, developed methodology to process the altimeter data using Matlab Software, Validated and Visualized the results. Xiaoli Deng provided the resources, supervised the present study, administrated the project, helped with the formal analysis of the methods and results, as well as funding acquisition. Both authors contributed to the manuscript writing, review and editing.

Declaration of Competing Interest

None.

Acknowledgement

This research was supported by the Australian Research Council's Discovery Project funding scheme (project number DP150100615). The authors would like to thank AVISO+ and SARvatore for providing the Jason SGDR and Sentinel-3A products. The authors would also like to thank Professor Mark Stewart for proof reading of the paper and very helpful comments from the reviewers.

References

Abdalla, S., 2012. Ku-band radar altimeter surface wind speed algorithm. Mar. Geod. 35 (Sup 1), 276–298.
Ablain, M., Cazenave, A., Larnicol, G., Balmaseda, M., Cipollini, P., Faugère, Y., Fernandes, M.J., Henry, O., Johannessen, J.A., Knudsen, P., Andersen, O., 2015. Improved sea level record over the satellite altimetry era (1993–2010) from the climate change initiative project. Ocean Sci. 11 (1), 67–82.
Andersen, O., Rio, M.H., 2011. On the accuracy of current mean sea surface models for the use with GOCE data. In: 4th International GOCE User Workshop, pp. 696.
Andersen, O.B., Scharroo, R., 2011. Range and geophysical corrections in coastal regions: and implications for mean sea surface determination. In: Coastal Altimetry. Springer, pp. 103–145.
Birol, F., Delebecque, C., 2014. Using high sampling rate (10/20 Hz) altimeter data for the observation of coastal surface currents: a case study over the northwestern Mediterranean Sea. J. Mar. Syst. 129, 318–333.
Born, G.H., Richards, M.A., Rosborough, G.W., 1982. An empirical determination of the effects of sea state bias on SEASAT altimetry. J. Geophys. Res. Oceans 87 (C5), 3221–3226.
Bouffard, J., Roblou, L., Birol, F., Pascual, A., Fenoglio-Marc, L., Cancet, M., Morrow, R., Ménard, Y., 2011. Introduction and assessment of improved coastal altimetry strategies: case study over the Northwestern Mediterranean Sea. In: Coastal Altimetry. Springer, Berlin, Heidelberg, pp. 297–330.
Carrère, L., Lyard, F., 2003. Modeling the barotropic response of the global ocean to atmospheric wind and pressure forcing-comparisons with observations. Geophys. Res. Lett. 30 (6).
Cartwright, D.E., Tayler, R.J., 1971. New computations of the tide-generating potential. Geophys. J. Int. 23 (1), 45–73.
Cartwright, D.E., Edden, A.C., 1973. Corrected tables of tidal harmonics. Geophys. J. Int. 33 (3), 253–264.
Chelton, D.B., 1994. The sea state bias in altimeter estimates of sea level from collinear analysis of TOPEX data. J. Geophys. Res. Oceans 99 (C12), 24995–25008.
Cipollini, P., Benveniste, J., Birol, F., Fernandes, M., Obligis, E., Passaro, M., Strub, P., Valladeau, G., Vignudelli, S., Wilkin, J., 2017a. Satellite altimetry in coastal regions. In: Satellite Altimetry Over Oceans and Land Surfaces, pp. 343–380 New York.
Cipollini, P., Calafat, F.M., Jevrejeva, S., Melet, A., Prandi, P., 2017b. Monitoring sea level in the coastal zone with satellite altimetry and tide gauges. In: Integrative Study of the Mean Sea Level and Its Components. Springer, pp. 35–59.
Deng, X., Griffin, D.A., Ridgway, K., Church, J.A., Featherstone, W.E., White, N., Cahill, M., 2011. Satellite altimetry for geodetic, oceanographic, and climate studies in the Australian region. In: Coastal Altimetry. Springer, pp. 473–508.
Desportes, C., Obligis, E., Eymard, L., 2009. One-dimensional variational retrieval of the wet tropospheric correction for altimetry in coastal regions. IEEE Trans. Geosci. Remote Sens. 48 (3), 1001–1008.
Dinardo, S., Fenoglio-Marc, L., Buchhaupt, C., Becker, M., Scharroo, R., Fernandes, M.J., Benveniste, J., 2018. Coastal SAR and PLRM altimetry in German bight and West Baltic Sea. Adv. Space Res. 62 (6), 1371–1404.
Donlon, C., Berruti, B., Buongiorno, A., Ferreira, M.H., Féménias, P., Frerick, J., Goryl, P., Klein, U., Laur, H., Mavrocordatos, C., 2012. The global monitoring for environment and security (GMES) Sentinel-3 mission. Remote Sens. Environ. 120, 37–57.
Durand, F., Piecuch, C.G., Becker, M., Papa, F., Raju, S.V., Khan, J.U., Ponte, R.M., 2019. Impact of continental freshwater runoff on coastal sea level. Surv. Geophys. 40 (6), 1437–1466.
Fenoglio, L., Dinardo, S., Buchhaupt, C., Uebbing, B., Scharroo, R., Kusche, J., Benveniste, J., 2019. Calibrating CryoSat-2 and Sentinel-3A Sea Surface Heights along the German Coast.
Fernandes, M.J., Lázaro, C., 2016. GPD+ wet tropospheric corrections for CryoSat-2 and GFO altimetry missions. Remote Sens. 8 (10), 851.
Fernandes, M.J., Lázaro, C., Ablain, M., Pires, N., 2015. Improved wet path delays for all ESA and reference altimetric missions. Remote Sens. Environ. 169, 50–74.
Fu, L.-L., Glazman, R., 1991. The effect of the degree of wave development on the sea state bias in radar altimetry measurement. J. Geophys. Res. Oceans 96, 829–834.
Garcia, E.S., Sandwell, D.T., Smith, W.H., 2014. Retracking CryoSat-2, Envisat and Jason-1 radar altimetry waveforms for improved gravity field recovery. Geophys. J. Int. 196 (3), 1402–1422.
Gaspar, P., Florens, J.P., 1998. Estimation of the sea state bias in radar altimeter measurements of sea level: results from a new nonparametric method. J. Geophys. Res. Oceans 103 (C8), 15803–15814.
Gaspar, P., Ogor, F., Le Traon, P.Y., Zanife, O.Z., 1994. Estimating the sea state bias of the TOPEX and POSEIDON altimeters from crossover differences. J. Geophys. Res. Oceans 99 (C12), 24981–24994.
Gómez-Enri, J., González, C., Passaro, M., Vignudelli, S., Álvarez, O., Cipollini, P., Izquierdo, A., 2019. Wind-induced cross-strait sea level variability in the strait of Gibraltar from coastal altimetry and in-situ measurements. Remote Sens. Environ. 221, 596–608.
Gommenginger, C., Thibaut, P., Fenoglio-Marc, L., Quartly, G., Deng, X., Gómez-Enri, J., Gao, Y., 2011. Retracking altimeter waveforms near the coasts. In: Coastal Altimetry. Springer, pp. 61–101.
Hemer, M.A., Church, J.A., Hunter, J.R., 2007. Waves and climate change on the Australian coast. J. Coast. Res. 432–437.
Karimi, A.A., Deng, X., Andersen, O.B., 2019. Sea level variation around Australia and its relation to climate indices. Mar. Geod. 42 (5), 469–489. https://doi.org/10.1080/01490419.2019.1629131.
Labroue, S., Gaspar, P., Dorandeu, J., Mertz, F., Tran, N., Zanife, O.Z., Femenias, P., 2006. Overview of the improvements made on the empirical determination of the sea state bias correction. Am. J. Agric. Econ. 614, 77.
Labroue, S., Tran, N., Vandermark, D., Scharroo, R., Feng, H., 2008. Sea state bias correction in coastal waters. In: Second Coastal Altimetry Workshop, pp. 6–7 Pisa, Italy.
Labroue, S., Boy, F., Picot, N., Urvoy, M., Ablain, M., 2012. First quality assessment of the Cryosat-2 altimetric system over ocean. Adv. Space Res. 50 (8), 1030–1045.
McInnes, K.L., White, C.J., Haigh, I.D., Hemer, M.A., Hoeke, R.K., Holbrook, N.J., Kiem, A.S., Oliver, E.C., Ranasinghe, R., Walsh, K.J., Westra, S., 2016. Natural hazards in Australia: sea level and coastal extremes. Clim. Chang. 139 (1), 69–83.
Mercier, F., Picot, N., Guinle, T., Cazenave, A., Kosuth, P., Seyler, F., 2012. The PISTACH project for coastal and hydrology altimetry: 2012 project status and activities. In: Presentation at 20 Years of Progress in Radar Altimetry Symposium, (Venice, Italy).
Moreau, T., Tran, N., Aublanc, J., Tison, C., Le Gac, S., Boy, F., 2018. Impact of long ocean waves on wave height retrieval from SAR altimetry data. Adv. Space Res. 62 (6), 1434–1444.
Obligis, E., Desportes, C., Eymard, L., Fernandes, M.J., Lázaro, C., Nunes, A.L., 2011. Tropospheric corrections for coastal altimetry. In: Coastal Altimetry. Springer Berlin Heidelberg, pp. 147–176. https://doi.org/10.1007/978-3-642-12796-0_6.
Pascual, A., Marcos, M., Gomis, D., 2008. Comparing the sea level response to pressure and wind forcing of two barotropic models: validation with tide gauge and altimetry data. J. Geophys. Res. Oceans 113 (C7).
Passaro, M., Cipollini, P., Vignudelli, S., Quartly, G.D., Snaith, H.M., 2014. ALES: a multi-mission adaptive subwaveform retracker for coastal and open ocean altimetry. Remote Sens. Environ. 145, 173–189.
Passaro, M., Nadzir, Z.A., Quartly, G.D., 2018. Improving the precision of sea level data from satellite altimetry with high-frequency and regional sea state bias corrections. Remote Sens. Environ. 218, 245–254.
Peng, F., Deng, X., 2018a. A new retracking technique for Brown peaky altimetric waveforms. Mar. Geod. 41 (2), 99–125.
Peng, F., Deng, X., 2018b. Validation of improved SignificantWave heights from the Brown-Peaky (BP) Retracker along the East Coast of Australia. Remote Sens. 10 (7), 1072. https://doi.org/10.3390/rs10071072.
Peng, F., Deng, X., 2020. Validation of sentinel-3A SAR mode sea level anomalies around the Australian coastal region. Remote Sens. Environ. 237, 111548.
Pires, N., Fernandes, M.J., Gommenginger, C., Scharroo, R., 2016. A conceptually simple modeling approach for Jason-1 sea state bias correction based on 3 parameters exclusively derived from altimetric information. Remote Sens. 8 (7), 576.
Pujol, M.I., Schaeffer, P., Faugère, Y., Raynal, M., Dibarboure, G., Picot, N., 2018. Gauging the improvement of recent mean sea surface models: a new approach for identifying and quantifying their errors. J. Geophys. Res. Oceans 123 (8), 5889–5911.
Quartly, G.D., Smith, W.H., Passaro, M., 2019. Removing Intra-1-Hz covariant error to improve altimetric profiles of sigma0 and sea surface height. IEEE Trans. Geosci. Remote Sens. 57 (6), 3741–3752.
Ray, C., Martin-Puig, C., Clarizia, M.P., Ruffini, G., Dinardo, S., Gommenginger, C., Benveniste, J., 2014. SAR altimeter backscattered waveform model. IEEE Trans. Geosci. Remote Sens. 53 (2), 911–919.
Sandwell, D.T., Smith, W.H., 2005. Retracking ERS-1 altimeter waveforms for optimal gravity field recovery. Geophys. J. Int. 163 (1), 79–89.
Sandwell, D.T., Smith, W.H., Gille, S., Kappel, E., Jayne, S., Soofi, K., Coakley, B., Géli, L., 2006. Bathymetry from space: rationale and requirements for a new, high-resolution altimetric mission. Compt. Rendus Geosci. 338 (14–15), 1049–1062.
Schaeffer, P., Pujol, I., Faugere, Y., Guillot, A., Picot, N., 2016. The CNES CLS 2015 global mean sea surface. Presentation OSTST 2016.
Scharroo, R., Leuliette, E.W., Lillibridge, J.L., Byrne, D., Naeije, M.C., Mitchum, G.T., 2013, September. RADS: Consistent multi-mission products. In: Proc. of the Symposium on. 20. pp. 4.
Seifi, F., Deng, X., Baltazar Andersen, O., 2019. Assessment of the accuracy of recent empirical and assimilated tidal models for the great barrier reef, Australia, using satellite and coastal data. Remote Sens. 11 (10), 1211.
Stammer, D., Ray, R., Andersen, O.B., Arbic, B., Bosch, W., Carrère, L., Egbert, G., 2014. Accuracy assessment of global barotropic ocean tide models. Rev. Geophys. 52 (3),

243–282.
Tran, N., Vandemark, D., Chapron, B., Labroue, S., Feng, H., Beckley, B., Vincent, P., 2006. New models for satellite altimeter sea state bias correction developed using global wave model data. J. Geophys. Res. Oceans 111 (C9).
Tran, N., Labroue, S., Philipps, S., Bronner, E., Picot, N., 2010a. Overview and update of the sea state bias corrections for the Jason-2, Jason-1 and TOPEX missions. Mar. Geod. 33 (S1), 348–362.
Tran, N., Vandemark, D., Labroue, S., Feng, H., Chapron, B., Tolman, H., Picot, N., 2010b. Sea state bias in altimeter sea level estimates determined by combining wave model and satellite data. J. Geophys. Res. Oceans 115 (C3).
Tran, N., Philipps, S., Poisson, J.C., Urien, S., Bronner, E., Picot, N., 2012, September. Impact of GDR_D standards on SSB corrections. In: Ocean Science Topography Science Team Meeting, (Venice).
Vandemark, D., Tran, N., Beckley, B., Chapron, B., Gaspar, P., 2002. Direct estimation of sea state impacts on radar altimeter sea level measurements. Geophys. Res. Lett. 29 (24), 11–14.
Wahr, J.M., 1985. Deformation induced by polar motion. J. Geophys. Res. Solid Earth 90 (B11), 9363–9368.
Zaron, E.D., DeCarvalho, R., 2016. Identification and reduction of retracker-related noise in altimeter-derived sea surface height measurements. J. Atmos. Ocean. Technol. 33 (1), 201–210.